Double-pulse laser illumination method for measuring fast cerebral blood flow velocities in the deep brain using a fiber-bundle-based endomicroscopy system

MINKYUNG KIM,[1,2] JINKI HONG,[1,2] AND HYUN-JOON SHIN[1,2,*]

[1]*Center for Bionics, Biomedical Research Institute, Korea Institute of Science and Technology, Seoul 02792, South Korea*
[2]*Biomedical Engineering, KIST School, UST, Korea University of Science and Technology, Seoul 02792, South Korea*
[*]kaiphy@kist.re.kr

Abstract: We present a new fiber-bundle-based endomicroscopy system to measure the fast cerebral blood flow (CBF) velocity in blood vessels located between the surface and the deep brain of living animals. The CBF velocity is obtained by measuring the displacement of the partially overlapped red blood cell images directly, using double-pulse 532-nm laser illumination. The proposed method could measure CBF in blood vessels with diameters ranging from 4 μm to 42 μm and could measure CBF velocities up to 3.2 μm/ms for different vessel diameters at a depth of 2.1 mm from the brain surface in a living mouse.

References and links

1. P. Venkat, M. Chopp, and J. Chen, "New insights into coupling and uncoupling of cerebral blood flow and metabolism in the brain," Croat. Med. J. **57**(3), 223–228 (2016).
2. I. F. Kimbrough, S. Robel, E. D. Roberson, and H. Sontheimer, "Vascular amyloidosis impairs the gliovascular unit in a mouse model of Alzheimer's disease," Brain **138**(12), 3716–3733 (2015).
3. V. Berezowski, A. M. Fukuda, R. Cecchelli, and J. Badaut, "Endothelial Cells and Astrocytes: A Concerto en Duo in Ischemic Pathophysiology," Int. J. Cell Biol. **2012**, 176287 (2012).
4. D. A. Turner and D. C. Adamson, "Neuronal-Astrocyte Metabolic Interactions: Understanding the Transition into Abnormal Astrocytoma Metabolism," J. Neuropathol. Exp. Neurol. **70**(3), 167–176 (2011).
5. P. J. Magistretti and I. Allaman, "A Cellular Perspective on Brain Energy Metabolism and Functional Imaging," Neuron **86**(4), 883–901 (2015).
6. R. Oliveira, S. Semedo, E. Figueiras, L. F. R. Ferreira, and A. Humeau, "Laser Doppler flowmeters for microcirculation measurements," in 1st Portuguese Biomedical Engineering Meeting, 2011), 1–4.
7. T. O. Manning, N. A. Monteiro-Riviere, D. G. Bristol, and J. E. Riviere, "Cutaneous laser-Doppler velocimetry in nine animal species," Am. J. Vet. Res. **52**(12), 1960–1964 (1991).
8. H. Cheng, Q. Luo, Q. Liu, Q. Lu, H. Gong, and S. Zeng, "Laser speckle imaging of blood flow in microcirculation," Phys. Med. Biol. **49**(7), 1347–1357 (2004).
9. S. M. S. Kazmi, A. B. Parthasarthy, N. E. Song, T. A. Jones, and A. K. Dunn, "Chronic imaging of cortical blood flow using Multi-Exposure Speckle Imaging," J. Cereb. Blood Flow Metab. **33**(6), 798–808 (2013).
10. M. E. Secchi, A. Sulli, C. Pizzorni, and M. Cutolo, "Studio della microangiopatia sclerodermia mediante valutazione dinamica con laser-Doppler e morfologica con videocapillaroscopia periungueale: risultati preliminari.," Reumatismo **61**(1), 34–40 (2009).
11. M. Tomita, T. Osada, I. Schiszler, Y. Tomita, M. Unekawa, H. Toriumi, N. Tanahashi, and N. Suzuki, "Automated Method for Tracking Vast Numbers of FITC-Labeled RBCs in Microvessels of Rat Brain in Vivo Using a High-Speed Confocal Microscope System," Microcirculation **15**(2), 163–174 (2008).
12. M. Unekawa, M. Tomita, T. Osade, Y. Tomita, H. Toriumi, J. Tatarishvili, and N. Suzuki, "Frequency distribution function of red blood cell velocities in single capillaries of the rat cerebral cortex using intravital laser-scanning confocal microscopy with high-speed camera," Asian Biomed. **2**, 203–218 (2008).
13. R. Hoshikawa, H. Kawaguchi, H. Takuwa, Y. Ikoma, Y. Tomita, M. Unekawa, N. Suzuki, I. Kanno, and K. Masamoto, "Dynamic Flow Velocity Mapping from Fluorescent Dye Transit Times in the Brain Surface Microcirculation of Anesthetized Rats and Mice," Microcirculation **23**(6), 416–425 (2016).
14. D. Kleinfeld, P. P. Mitra, F. Helmchen, and W. Denk, "Fluctuations and stimulus-induced changes in blood flow observed in individual capillaries in layers 2 through 4 of rat neocortex," Proc. Natl. Acad. Sci. U.S.A. **95**(26), 15741–15746 (1998).

15. R. L. Rungta, B.-F. Osmanski, D. Boido, M. Tanter, and S. Charpak, "Light controls cerebral blood flow in naive animals," Nat. Commun. **8**, 14191 (2017).
16. P. Vérant, R. Serduc, B. Van Der Sanden, C. Rémy, and J. C. Vial, "A direct method for measuring mouse capillary cortical blood volume using multiphoton laser scanning microscopy," J. Cereb. Blood Flow Metab. **27**(5), 1072–1081 (2007).
17. A. Letourneur, V. Chen, G. Waterman, and P. J. Drew, "A method for longitudinal, transcranial imaging of blood flow and remodeling of the cerebral vasculature in postnatal mice," Physiol. Rep. **2**(12), 2 (2014).
18. W. Gao, "Quantitative depth resolved microcirculation imaging with optical coherence tomography angiography (Part II): Microvascular network imaging," Microcirculation doi: 10.1111/micc.12376 (2017).
19. V. Gradinaru, M. Mogri, K. R. Thompson, J. M. Henderson, and K. Deisseroth, "Optical deconstruction of parkinsonian neural circuitry," Science **324**(5925), 354–359 (2009).
20. B. Rosengarten, V. Dannhardt, O. Burr, M. Pöhler, S. Rosengarten, M. Oechsner, and I. Reuter, "Neurovascular Coupling in Parkinson's Disease Patients: Effects of Dementia and Acetylcholinesterase Inhibitor Treatment," J. Alzheimers Dis. **22**(2), 415–421 (2010).
21. M. Kim, J. Hong, J. Kim, and H. J. Shin, "Fiber bundle-based integrated platform for wide-field fluorescence imaging and patterned optical stimulation for modulation of vasoconstriction in the deep brain of a living animal," Biomed. Opt. Express **8**(6), 2781–2795 (2017).
22. T.-C. Huang, W.-C. Lin, C.-C. Wu, G. Zhang, and K.-P. Lin, "Experimental estimation of blood flow velocity through simulation of intravital microscopic imaging in micro-vessels by different image processing methods," Microvasc. Res. **80**(3), 477–483 (2010).
23. K. Masamoto, R. Hoshikawa, and H. Kawaguchi, "Fluorescence Imaging of Blood Flow Velocity in the Rodent Brain," Curr. Top. Med. Chem. **16**(24), 2677–2684 (2016).
24. M. Tomita, Y. Tomita, M. Unekawa, H. Toriumi, and N. Suzuki, "Oscillating neuro-capillary coupling during cortical spreading depression as observed by tracking of FITC-labeled RBCs in single capillaries," Neuroimage **56**(3), 1001–1010 (2011).
25. M. A. Kurochkin, E. S. Stiukhina, I. V. Fedosov, D. E. Postnov, and V. V. Tuchin, "Micro-PIV quantification of capillary blood flow redistribution caused by laser-assisted vascular occlusion," Proc. SPIE, **9917**, 9917 (2016).
26. C. E. Willert and M. Gharib, "Digital particle image velocimetry," Exp. Fluids **10**(4), 181–193 (1991).
27. K. Jambunathan, X. Y. Ju, B. N. Dobbins, and S. Ashforth-Frost, "An improved cross correlation technique for particle image velocimetry," Meas. Sci. Technol. **6**(5), 507–514 (1995).
28. A. G. Koutsiaris, D. S. Mathioulakis, and S. Tsangaris, "Microscope PIV for velocity-field measurement of particle suspensions flowing inside glass capillaries," Meas. Sci. Technol. **10**(11), 1037–1046 (1999).
29. J. Soria, "An investigation of the near wake of a circular cylinder using a video-based digital cross-correlation particle image velocimetry technique," Exp. Therm. Fluid Sci. **12**(2), 221–233 (1996).
30. R. J. Adrian, "Image shifting technique to resolve directional ambiguity in double-pulsed velocity," Appl. Opt. **25**(21), 3855–3858 (1986).
31. A. Vogel and W. Lauterborn, "Time-Resolved Particle Image Velocimetry Used in the Investigation of Cavitation Bubble Dynamics," Appl. Opt. **27**(9), 1869–1876 (1988).
32. Z. C. Liu, C. C. Landreth, R. J. Adrian, and T. J. Hanratty, "High-Resolution Measurement of Turbulent Structure in a Channel with Particle Image Velocimetry," Exp. Fluids **10**(6), 301–312 (1991).
33. A. Cenedese and A. Paglialunga, "Digital Direct Analysis of a Multiexposed Photograph in Piv," Exp. Fluids **8**(5), 273–280 (1990).
34. Y. Sugii, S. Nishio, and K. Okamoto, "In vivo PIV measurement of red blood cell velocity field in microvessels considering mesentery motion," Physiol. Meas. **23**(2), 403–416 (2002).
35. W.-H. Kim, C.-I. Kim, S.-W. Lee, S.-H. Lim, C.-W. Park, H. Lee, and M.-K. Park, "Particle Image Velocimetry of the Blood Flow in a Micro-channel Using the Confocal Laser Scanning Microscope," J. Opt. Soc. Korea **14**(1), 42–48 (2010).
36. S. Nakamura, D. W. Walker, and F. Y. Wong, "Cerebral haemodynamic response to somatosensory stimulation in near-term fetal sheep," J. Physiol. **595**(4), 1289–1303 (2017).
37. L. Krizanac-Bengez, M. R. Mayberg, and D. Janigro, "The cerebral vasculature as a therapeutic target for neurological disorders and the role of shear stress in vascular homeostatis and pathophysiology," Neurol. Res. **26**(8), 846–853 (2004).
38. K. B. J. Franklin and G. Paxinos, *The Mouse Brain in Stereotaxic Coordinates* (Academic Press, 1997), pp. xxii p., 186 p. of plates.
39. T. N. Ford, D. Lim, and J. Mertz, "Fast optically sectioned fluorescence HiLo endomicroscopy," J. Biomed. Opt. **17**(2), 021105 (2012).
40. D. W. Slaaf, T. J. M. Jeurens, G. J. Tangelder, R. S. Reneman, and T. Arts, "Methods to measure blood flow velocity of red blood cells in vivo at the microscopic level," Ann. Biomed. Eng. **14**(2), 175–186 (1986).
41. J. H. Park, J. K. Hong, J. Y. Jang, J. An, K. S. Lee, T. M. Kang, H. J. Shin, and J. F. Suh, "Optogenetic Modulation of Urinary Bladder Contraction for Lower Urinary Tract Dysfunction," Sci. Rep. **7**, 40872 (2017).
42. C. Iadecola, "Neurovascular regulation in the normal brain and in Alzheimer's disease," Nat. Rev. Neurosci. **5**(5), 347–360 (2004).
43. Y. Mandel, R. Manivanh, R. Dalal, P. Huie, J. Wang, M. Brinton, and D. Palanker, "Vasoconstriction by electrical stimulation: new approach to control of non-compressible hemorrhage," Sci. Rep. **3**(1), 2111 (2013).
44. E. G. Lakatta and D. Levy, "Arterial and cardiac aging: major shareholders in cardiovascular disease enterprises: Part I: aging arteries: a "set up" for vascular disease," Circulation **107**(1), 139–146 (2003).
45. R. H. Mohiaddin, D. N. Firmin, and D. B. Longmore, "Age-related changes of human aortic flow wave velocity measured noninvasively by magnetic resonance imaging," J. Appl. Physiol. **74**(1), 492–497 (1993).

46. O. Yizhar, L. E. Fenno, T. J. Davidson, M. Mogri, K. Deisseroth, J. Tolo, A. Gordus, M. B. Orger, K. E. Severi, J. J. Macklin, R. Patel, S. R. Pulver, T. J. Wardill, E. Fischer, C. Schuler, T. W. Chen, K. S. Sarkisyan, J. S. Marvin, C. I. Bargmann, D. S. Kim, S. Kugler, L. Lagnado, P. Hegemann, A. Gottschalk, E. R. Schreiter, and L. L. Looger, "Optogenetics in neural systems," Neuron **71**(1), 9–34 (2011).
47. O. Yizhar, L. E. Fenno, T. J. Davidson, M. Mogri, and K. Deisseroth, "Optogenetics in neural systems," Neuron **71**(1), 9–34 (2011).

1. Introduction

Circulating cerebral blood transports products such as oxygen, nutrients, and blood-mediated messengers to brain and removes waste from the brain tissues, depending on the neuronal requirements [1]. The exchange of these products between blood and brain tissue occurs at the microcirculation level. Therefore, mapping microcirculations such as blood flows and vascular distributions in the brains of living animals is important for understanding the functional activities of the neurovascular and gliovascular units [2, 3]. Functional changes in cellular-level interactions alter brain activity, hemodynamics, and metabolism, by regulating multiple physiological pathways at the systemic and local levels [4, 5]. Therefore, the measurement of the functional status and, in particular, the dynamics of the current microcirculatory network provides important information for researchers and clinicians. This is why various techniques are being developed to measure the spatiotemporal patterns of cerebral microcirculation.

Laser doppler flowmetry [6], laser doppler velocimetry [7], laser speckle contrast analysis, and diffusing-wave spectroscopy are blood-flow measurement techniques commonly used to analyze the microcirculation of blood [8–10]. Recently, optical coherent angiography and confocal and two-photon laser scanning microscopy have been widely applied to the development of cerebral blood flow (CBF) measurement systems [11–17]. However, each technique has its own limitations. The pointwise measurement methods such as laser doppler flowmetry and laser doppler velocimetry are unable to calculate the blood-flow velocity distribution throughout the microscope field of view, and laser speckle contrast analysis and diffusing-wave spectroscopy can only measure relative flow changes. Furthermore, these methods are unsuitable for measuring the changes in vessel diameters or the interconnections between neurons. Two- or three-dimensional imaging techniques such as optical coherent angiography or laser scanning microscopy have been applied to a variety of CBF studies because they can obtain a variety of image information at individual cell levels, with high spatial resolutions [15, 18]. However, such a high spatial resolution measurement technique has a disadvantage in that it takes a considerable amount of time to acquire the information of the whole blood vessel distributed over the entire field of view. In addition, it requires effort to overcome the limited penetration depth of brain tissue [19, 20].

Intravital-microscopy is a powerful alternative to in vivo brain imaging and biomechanical analysis [12, 21, 22]. We had previously introduced a fiber-bundle-based integrated platform of the intravital-fluorescence-microscopy type for in vivo brain study [21]. The optical platform could real-time fluorescence imaging with high spatiotemporal resolution, when inserted directly into a mouse's brain, while simultaneously stimulating vasoconstriction optically. However, this optical platform was based on an epifluorescence microscope that used a relatively low-frame-rate (e.g., 10 frames per second (fps) or less) charge-coupled device (CCD) camera and broad-band light source with long exposure time (e.g., 100 ms or more). Such low-frame-rate imaging systems are not suitable for experiments that require high frame rates, such as fast blood flow measurements, because they can miss the flow of high-speed red blood cells (RBCs).

Two methods can be integrated into an optical platform for high-speed CBF measurements: (i) high-speed imaging method [11–13, 23,24] and (ii) micro particle image velocimetry (μ-PIV) method [25–28].

A high-speed imaging system can measure fast blood cell movement by using higher-temporal-resolution image-acquisition equipment such as a high-frame-rate video camera (e.g., 500 fps) [11, 12, 24].

However, the high-speed imaging system is not suitable for the simultaneous measurement of high-resolution images of the changes in neuronal activity and structures around the blood vessels during blood-flow measurement. Furthermore, its measurable range is limited by the performance of the camera used. Thus, to obtain a variety of imaging information, additional measuring devices with various frame rates or resolutions may be required, resulting in an economic burden and increasing the system size [24].

On the other hand, µ-PIV is a quantitative flow visualization method, which can be used to measure full-field velocity data within a two-dimensional (2D) plane of a particle-seeded flow field, such as the turbulent wake of a cylinder [29], jets in the water, or the flow around cavitation bubbles [30, 31]. In double or multiple exposure images of PIV, images of the flow field are recorded on the film and various techniques are used to extract the velocity data [9, 32, 33]. The combination of a PIV and a microscope increases the resolution of conventional PIVs and can be used in microcirculation to measure velocities in small-sized vessels or for velocity measurements in other applications [25, 28, 34, 35]. It can change the system flexibly depending on the situation by replacing or adding the laser source of an existing microscope system. By adjusting various system parameters such as laser pulse widths and laser intervals, it can measure various velocities over a wide range of image conditions without adding supplementary high-frame-rate devices or increasing the system size.

However, this technique has not yet been applied to velocity measurement using intravital-microscopy in cerebral vessels of living animals.

We therefore applied this latter method to the fiber-bundle-based integrated platform. We developed a new optical platform for measuring the two-dimensional image of CBF in living animals by combining the PIV technique with the previously developed intravital-microscopy–type fiber-bundle-based integrated platform. In the present study, the new fiber-bundle-based microscope-PIV integrated platform is used to image cerebral blood vessels on the surface or deep brain of anesthetized mice and to obtain a CBF velocity map of the entire platform field of view. Our experimental results demonstrate that the proposed technique can be a promising tool for studying cerebrovascular diseases or hemodynamics in live-animal functional unit connections [1–3, 36, 37].
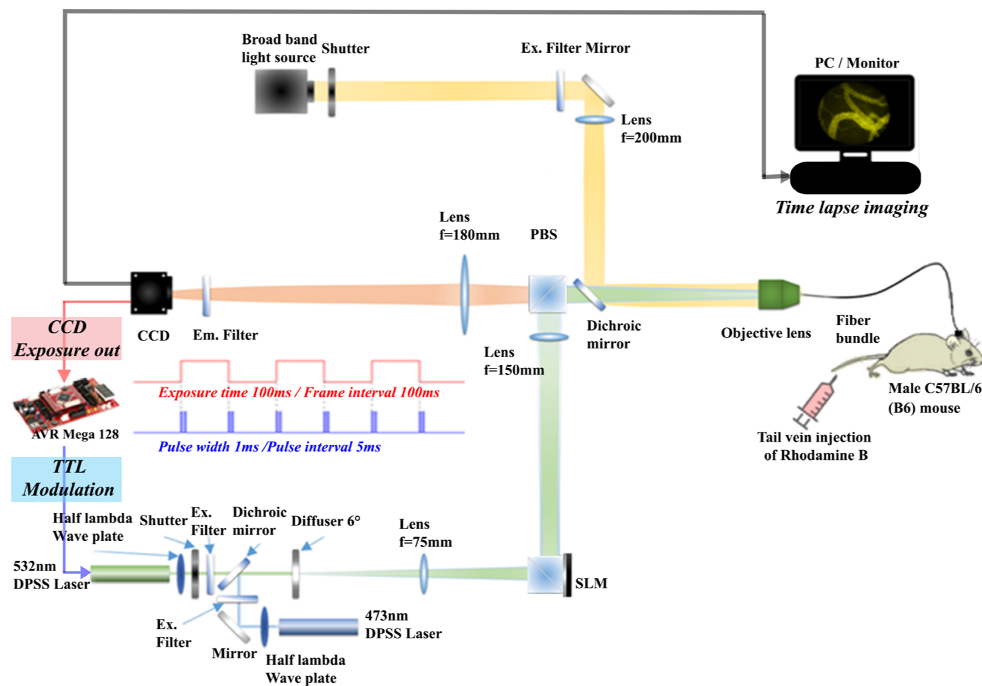
Fig. 1. Schematic diagram of in-vivo fiber-bundle-based endomicroscopy system. It combines an optical platform with a fiber-bundle-based integrated platform and a double pulse laser illumination system using a 300mW 532-nm diode pumped solid state (DPSS) continuous wave (C.W.) laser and Atmega128 microcontroller. Abbreviations: PBS: polarizing beam splitter, SLM: spatial light modulator.

2. Methods

2.1 Fiber-bundle-based endomicroscopy system setup

To measure the velocity of fast CBF, we combined our previously developed fiber-bundle-based integrated fluorescence imaging platform with a double-pulse 532-nm laser illumination system (Fig. 1). The principle and detailed configuration of our previously developed optical platform can be found in our previous work [21].

In brief, the fiber-bundle-based integrated platform is composed of three components: (i) a multicolor fluorescent light illumination part, (ii) a wide-field fluorescence imaging part, and (iii) a patterned 473-nm light stimulation part. In the previous platform, a reflective spatial light modulator (SLM; LC-R720, amplitude modulation, Holoeye) was used to create 473-nm laser light patterns for the real-time patterned optical stimulation of brain structures for optogenetics. The 473-nm laser and a broad-band lamp was used for the fluorescent microscope imaging of brain structures of various sizes ranging from several micrometers to several hundreds of micrometers, such as blood vessels, neurons, and astrocytes. However, the existing light sources were not sufficient for the imaging of fast-flowing blood.

In the new optical platform, we added a 532-nm diode-pumped solid-state (DPSS) laser (MGL-III-532-300 mW, CNI Optoelectronics Tech. Co.) in the same path of the 473-nm DPSS laser (MBL-H-473-300 mW, CNI Optoelectronics Tech. Co.) for imaging fast blood flow with a single- or double-pulse laser illumination method. The 532-nm DPSS laser could also be used as a light source for the fluorescence imaging of plasma injected with Rhodamine B isothiocyanate–Dextran diluent (70 KDa, 20 mg in 0.2 ml saline, Merck KGaA.).

After passing through a laser filter (LD01-473/10-25, Semrock), the 473-nm laser light was reflected by a dichroic mirror (Di01-R488, Semrock), which changed the direction of the

laser light by 90°. On the other hand, the 532-nm laser light, excited by a laser filter (FF01-532/3-25, Semrock), passed through the dichroic mirror. The 473-nm laser light and 532-nm laser light propagated together to the laser speckle-reducing diffuser (LSR-3005-6D-VIS, Optotune) and achromatic doublet lens (f = 75 mm). The laser lights became spatially homogeneous and the speckle noises were removed by the laser speckle reducer. The laser beams then proceeded to the first polarizing beam splitter (PBS) (CCM1-PBS251/M, Thorlabs, Inc.) and the SLM was used to create laser light patterns for full-field or partial illumination. The laser patterns were projected onto the fiber bundle by the achromatic lens (f = 150 mm) and the objective lens (UPLFLN 20x, NA 0.5, Olympus Corp.). The magnification of the laser-patterned system was designed as 16.7, to cover the surface of the fiber bundle without degrading the spatial resolution of the fiber bundle. The polished bare fiber bundle projected the laser pattern onto the brain surface and simultaneously transferred the fluorescence emitted from the brain surface to the opposite side. In this research, we used a one-meter fiber bundle (IGN-037-100, Sumitomo) with a diameter of 330 μm and core-to-core distance of 2 μm.

2.2 Modulation of 532-nm DPSS continuous-wave laser for the double-pulse laser illumination method

Because the size of blood cells is larger than a few micrometers and the flow velocity is comparatively slow, a modulated continuous laser was used for imaging, instead of using the expensive and large q-switched lasers commonly used as PIV light sources. Since the 532-nm DPSS laser is a continuous wave (CW) laser, pulse modulation is required for dual or multiple exposures. The laser light was modulated by an Atmega128 microcontroller from AVR (8-bit, AB-M128-B, NEWTC). The microcontroller used the video signal from the CCD camera to control the laser driver. Using 5V TTL +/− modulation, the laser pulse was controlled to be activated during the frame exposure ON time of the CCD camera. The microcontroller system could control the number of pulses (single, double, or multiple), pulse width, and pulse interval.

As shown in the schematic diagram of Fig. 1, when the CCD camera operates at 5 fps (frame exposure time 100 ms, interval between frames 100 ms), it outputs double laser pulses of 1 ms pulse duration and 5 ms interval between two pulses whenever the exposure ON signal of the image starts. Parameters such as CCD camera exposure time, frame rate, laser pulse width, and laser pulse interval are determined by the variables such as dose and concentration of fluorescent material, measured blood-flow velocity, laser output, and CCD camera gain value. In this paper, all experiments used a 532-nm DPSS CW laser output intensity of 100 mW/mm^2 and a CCD camera gain of 1.

2.3 Animal surgeries and preparation

All animal experimental procedures were approved by the Institutional Animal Care and Use Committee of the Korea Institute of Science and Technology (KIST, 2017-078) and followed the guidelines of the Institutional Animal Care and Use Committee of KIST. The body temperature was maintained near 37 °C using a feedback-controlled heating pad.

We studied eight-week-old male C57BL/6 (B6) mice weighing 20–23 g. The mice were anesthetized with urethane (1.5 g/kg, i.p.). Thirty minutes before the experiment, blood serum was labeled by tail-vein injection of Rhodamine B isothiocyanate–Dextran diluted in phosphate-buffered saline (PBS, 20 mg/0.2 mL). Surgery was conducted after head fixation on a stereotaxic atlas (51730, Stoelting Co.). After a small craniotomy (approximately 1 mm), the dura was removed for the insertion of the imaging fiber bundle. Using X and Y stereotaxic coordinates, the fiber bundle was positioned over the area to be imaged. The coordinates of the craniotomy were as follows: the anterior–posterior (AP) was + 1.4 mm, the medial–lateral (ML) was 1 mm from the bregma. These stereotaxic coordinates were established by Franklin and Paxinos [38]. The fiber bundle was very smoothly in contact with the brain surface and was inserted carefully into the deep brain at an approximate rate of 100

µm/s for blood vessel images located in the deep brain. The fluorescence image was taken with a band-pass filter (FF01-593/40-25, Semrock, Inc.).

2.4 Imaging post-processing and image enhancement

In order to eliminate the pixelation and improve the image quality, we used the iterative segmentation–interpolation algorithm proposed by Ford, to interpolate the intensity of the cladding region using the intensity of the adjacent fiber core [21, 39]. The post-processing was implemented using MATLAB (The Math Works, Inc.). All images presented in this paper are images processed after the image post-processing. In addition, image enhancement was performed using 2D filters of Image-Pro Premier 9.1 (Media Cybernetics, Inc.) for better identification of RBCs from plasma and for reducing the background noise. The enhancement performed by the 2D filters included the following steps: flatten (background (BG) intensity: bright, object width: 15 pixel); sharpen (kernel size: 3×3, strength: 100, passes: 3); median (kernel size: 5×5, threshold: 10%, level: 6554, passes: 1).

Image-Pro Premier 9.1 was also used to coat a pseudo color. Adobe Photoshop CS6 was used to insert scale bars; animate the frame rate; combine image tiles into a mosaic; and rotate, crop, and adjust the color balance of the images.
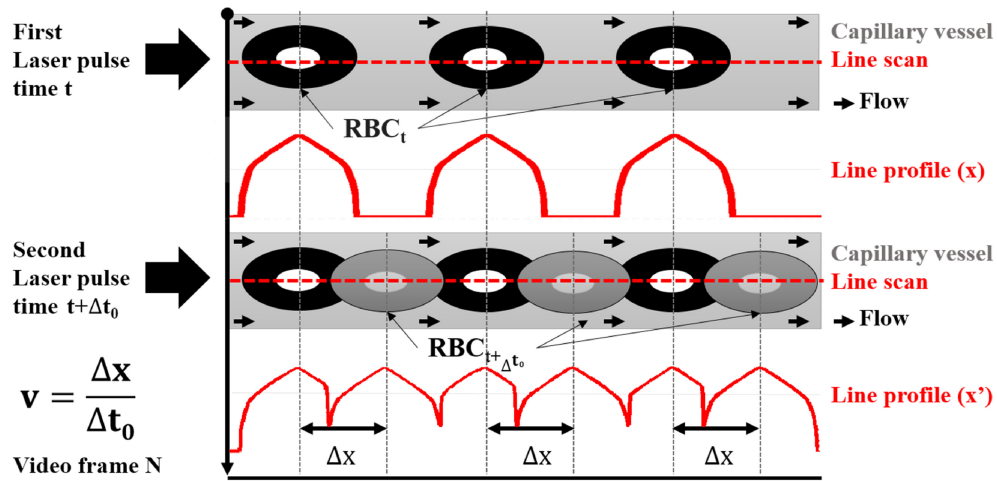

Fig. 2. Schematic representation of double-pulse laser illumination method. An illustration of the capillary is displayed. The line profile (**x**) is the relative fluorescence intensity measured along a scan line of red dashed line through the center of capillary to determine the position of RBCs in an image obtained using a single-pulse laser illumination with a pulse duration of t. And the line profile (**x**') is the relative fluorescence intensity measured under the double-pulse laser illumination at the same frame. Δt_0 is the time interval between the first and the second laser pulse. The displacement of individual RBCs during the pulse interval time yields the displacement difference (Δ**x**). RBC_t is the RBC image captured in the first laser pulse. $RBC_{t+\Delta t0}$ is the RBC image captured in the second laser pulse. In this illustration, the RBCs show fluorescence intensity brighter than the plasma.

2.5 Data analysis

As shown in Fig. 2, the method of double-pulse laser illumination relied on sampling the displacement of the intensity signal along the double-pulse interval in the same frame. In the double-pulse laser illumination method, we compare the density patterns of RBCs with fluorescence-labeled plasma spacing of capillary vessels in video frames to obtain optimal correlations and evaluate the spatial movement Δ**x** that occurs during the time interval Δt_0. Thus, Δ**x** is the displacement difference between RBC_t and $RBC_{t+\Delta t0}$ in the fluorescence image obtained using the double-pulse laser illumination, where RBC_t is the RBC image captured in the first laser pulse, and $RBC_{t+\Delta t0}$ is the RBC image captured in the second laser

pulse. In order to obtain accurate double-pulse laser illumination video images, short dual-pulse laser light should be provided during the exposure of the video signal. It allows displacement measurement of partially overlapping RBC images by double-pulsed laser exposure. The velocity (v) can be calculated according to the formula:

$$v = \Delta x \,/\, \Delta t_0 \qquad\qquad (1)$$

where $\Delta \mathbf{x}$ is the displacement difference and Δt_0 is a certain preset interval.

We applied a tracking technology that measured the speed based on pairs of partially overlapping RBC in fluorescent CBF images by double-pulsed laser exposure. Autocorrelation and statistical tests were performed with OriginPro 8 (OriginLab Corp.) and Microsoft Excel (Microsoft). All values are mean ± standard deviation (SD) unless otherwise noted.

The displacement was found using autocorrelation of the spatial signal (Fig. 5(F)).
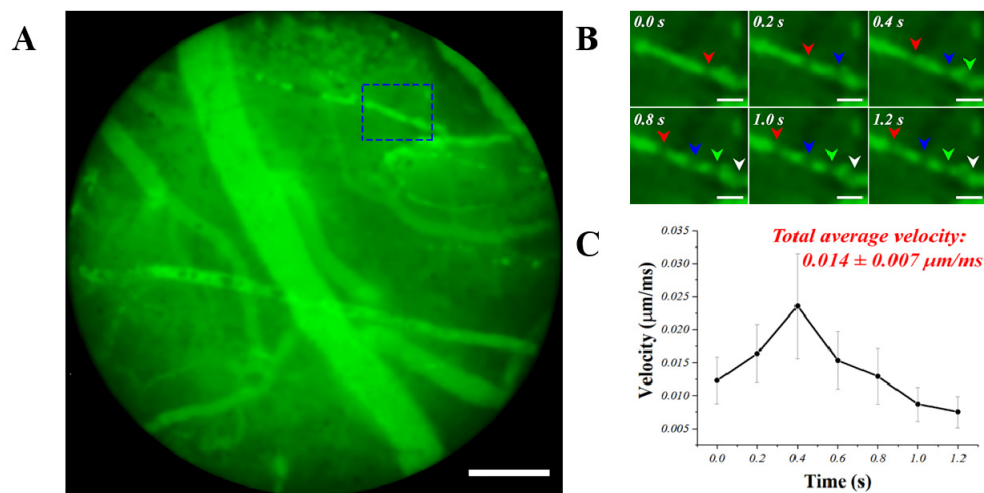

Fig. 3. Real-time fluorescent cerebrovascular image using a previously developed fiber-bundle-based integrated platform. (A) Blood-vessel imaging of the brain surface. (B) Cropped and magnified image sequence of the blue dashed box region in the image A. The red, blue, green, and white arrowheads indicate individual RBCs. (**C**) Calculated velocity chart plotted against time. Frame rate was 5 fps, and the exposure time was 200 ms. Illumination light output intensity was 1.2 mW/mm^2. Scale bars: (A) 100 μm, (B) 20 μm.

3. Results

3.1 Measurement of slow CBF in capillaries using the single-pulse laser illumination method

In the previous study, real-time fluorescence imaging of blood vessels was performed using avertin (250 mg/kg)-anesthetized live mice injected intravenously with a 200-μL bolus of fluorescein isothiocyanate (FITC)-dextran diluent. The fluorescence blood vessel images were taken with green fluorescent protein (GFP) band-pass filters (FF02-482/18-25, FF03-525/50-25, Semrock) at the frame rate of 5 fps. We could observe the flow of RBCs within capillaries of 9-μm diameter by visualizing the dark features, because the unlabeled RBCs appeared dark against the brighter background of the FITC dye mixed with the blood plasma, as shown in Fig. 3(A) and 3(B), and Visualization 1. The averaged blood-flow velocity for 1.2 s was measured as 0.014 ± 0.007 μm/ms.

These results demonstrate that the old optical platform using a single-pulse laser illumination could measure the slow blood flow. However, the velocity of 0.014 μm/ms was considerably slower than the mean value of RBC velocity in the cerebral capillaries of rodents, reported in other studies, which ranged from 0.39 to 2.08 μm/ms [12]. We were able

to measure the blood-flow velocities in capillaries up to 9-µm diameter only and it was difficult to measure the blood flow in larger blood vessels. In larger blood vessels, fast blood flow and dense particles such as RBCs and fluorescence molecules in plasma made it difficult to visualize and track RBCs that appeared as dark spots in low-speed frame-rate imaging. Therefore, to measure fast blood flow in larger vessels, a new measurement system is needed to capture the movement of the fast RBCs.

For this reason, we developed a new fiber-bundle-based microscope-PIV integrated platform that could measure fast CBFs in vessels of various diameters in the mouse brain. In all subsequent experiments, the blood flow has been measured using the new platform.
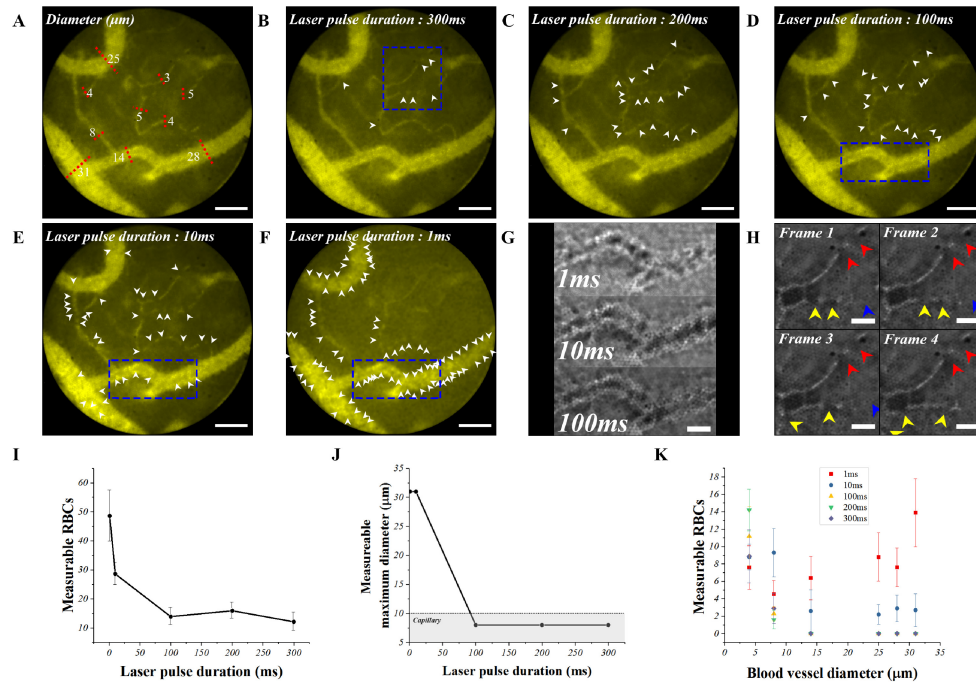

Fig. 4. Comparison of individual RBCs tracking ability according to laser pulse durations of single-pulse laser illumination method. (A) Distribution of blood vessel diameter on the brain surface. (B–F) Single-frame capture of fluorescent cerebrovascular imaging in the same area acquired using a single laser pulse with various laser pulse durations. White arrowheads indicate individual RBCs. (B) Laser pulse duration of 300 ms (see Visualization 2). (C) Laser pulse duration of 200 ms (see Visualization 3). (D) Laser pulse duration of 100 ms (see Visualization 4), (E) Laser pulse duration of 10 ms (see Visualization 5). (F) Laser pulse duration of 1 ms (see Visualization 6). (G) Cropped, magnified and enhanced images of the region in the blue dashed box in D–F for comparison. (H) Cropped, magnified and enhanced image sequence of the region in the blue dashed box in B. The red, yellow and blue arrowheads indicate individual RBCs. Red arrowheads: 'stagnant flow', yellow arrowheads: 'smooth flow', and blue arrowheads: 'clustering'. (I–K) The average number of RBCs was collected from 10 frames. (I) The average number of measurable RBCs according to laser pulse duration. (J) Measurable maximum diameter of cerebral vessels according to laser pulse duration. The gray box indicates the diameter range of the capillary. (K) The average number of measurable RBCs according to blood vessel diameter and laser pulse duration. Exposure time was matched to the duration of each laser pulse except for 1 ms laser pulse duration. When the laser pulse duration was 1ms, the exposure time was 10 ms. Frame interval was 100 ms, and 532-nm laser output intensity was 100 mW/mm². Scale bars: (A–F) 50 µm, (G, H) 20 µm.

3.2 Comparison of fluorescent CBF images obtained through the single-pulse laser illumination method with various pulse durations

To determine an appropriate laser pulse duration, we compared the RBC tracking ability, which changes with a series of exposure laser durations used to obtain fluorescent CBF images using the new platform, before measuring the blood-flow velocity. This experiment was performed on the assumption that the RBC tracking ability in an image obtained with a relatively short light exposure would be better than that in an image obtained with a long light exposure. Before the experiments, we injected Rhodamine B isothiocyanate–Dextran diluent (R9379, 70 KDa, Merck KGaA., 20 mg/0.2 ml) through a vein in the tail of the urethane-anesthetized mouse (1.5 g/kg, i.p.). The number of RBCs detected was measured for 300 ms, 200 ms, 100 ms, 10 ms, and 1 ms laser pulse durations using 10 fluorescence image sequences in six vessels with diameters ranging from 4 to 31 μm in the same brain region (Fig. 4(A)). The exposure time of the CCD camera matched the duration of the laser pulses, except for the 1 ms laser pulse. When the laser pulse duration was 1 ms, the exposure time was 10 ms.

All experiments were performed using a 100 ms frame interval and a 532-nm laser output intensity of 100 mW/mm^2. The fluorescence images were enhanced using the 2D filter of Image-Pro Premier 9.1, to improve the contrast between the blood vessels and the surrounding tissues and that between the RBCs and blood plasma to facilitate RBC tracking. This image enhancement process was performed on all fluorescence images for blood-flow velocity measurement. We also marked each individual RBC represented by black dots on bright plasma using white arrowheads.

As shown in the fluorescent CBF images (Fig. 4(B–F)), the number of measureable RBCs increased with decrease in the laser pulse duration: 12 ± 3 for 300 ms, 16 ± 3 for 200 ms, 14 ± 3 for 100 ms, 29 ± 4 for 10 ms, and 49 ± 9 for 1 ms (Fig. 4(I)). When the laser pulse duration was reduced from 300 ms to 1 ms, the measurable RBCs increased four times.

When comparing the enhanced fluorescence images obtained at laser pulse durations of 100 ms, 10 ms, and 1 ms in vessels located in the same region of interest (ROI), the individual RBCs could be observed more clearly, as black spots, as the pulse duration decreased from 100 ms to 1 ms (Fig. 4(G)).

As shown in Fig. 4(H), the RBC movements can be classified into three types: (i) "Stagnant flow": RBCs display no change in frame-to-frame movements, and are indicated by red arrowheads. (ii) "Smooth flow": RBCs have normal smooth flow, and are indicated by yellow arrowheads. (iii) "Clustering": These are displayed as large areas of dark features, which can be other floating substances without fluorescent labels in the blood vessels. These are indicated by blue arrowheads. The blood-flow velocities were measured by tracking only RBC movements corresponding to the "smooth flow", i.e., the second category.

We compared the maximum diameters of the blood vessels in which RBCs could be distinguished by changing the laser pulse duration (Fig. 4(J)). The RBCs were distinguished individually only in capillaries of diameters less than 10 μm in the fluorescence blood vessel images obtained using laser pulse durations ranging from 300 ms, 200 ms and 100 ms. On the other hand, in the fluorescence images obtained using laser pulse durations of 10 ms and 1 ms, individual RBCs could be identified in all blood vessels with diameters ranging from 4 μm to 31 μm, across the entire field of view. In addition, different laser pulse durations were used to compare the number of measurable RBCs in each vessel diameter (Fig. 4(K)).

The laser pulse durations that counted the maximum number of RBCs for each vessel diameter were: 4 μm: 14 ± 2 for 200 ms, 8 μm: 9 ± 3 for 10 ms, 14 μm: 6 ± 3 for 1 ms, 25 μm: 9 ± 3 for 1 ms, 28 μm: 8 ± 2 for 1 ms, and 31 μm: 14 ± 4 for 1 ms.

In particular, the average number of distinctive RBCs (n_{avg}) counted in the 4 μm capillary was the maximum for a laser pulse duration of 200 ms ($n_{avg} = 14 \pm 2$) and minimum for a laser pulse duration of 1 ms ($n_{avg} = 9 \pm 3$).

We tried to use a laser pulse duration of less than 1 ms; however, it is not shown in the results because the intensity of the laser was not large enough for fluorescence imaging of capillaries with diameters less than 10 μm. Based on these results, we selected a laser pulse

duration of 1 ms, which is suitable for measuring the movement of RBCs in 4-μm diameter capillaries and 31-μm diameter large vessels.
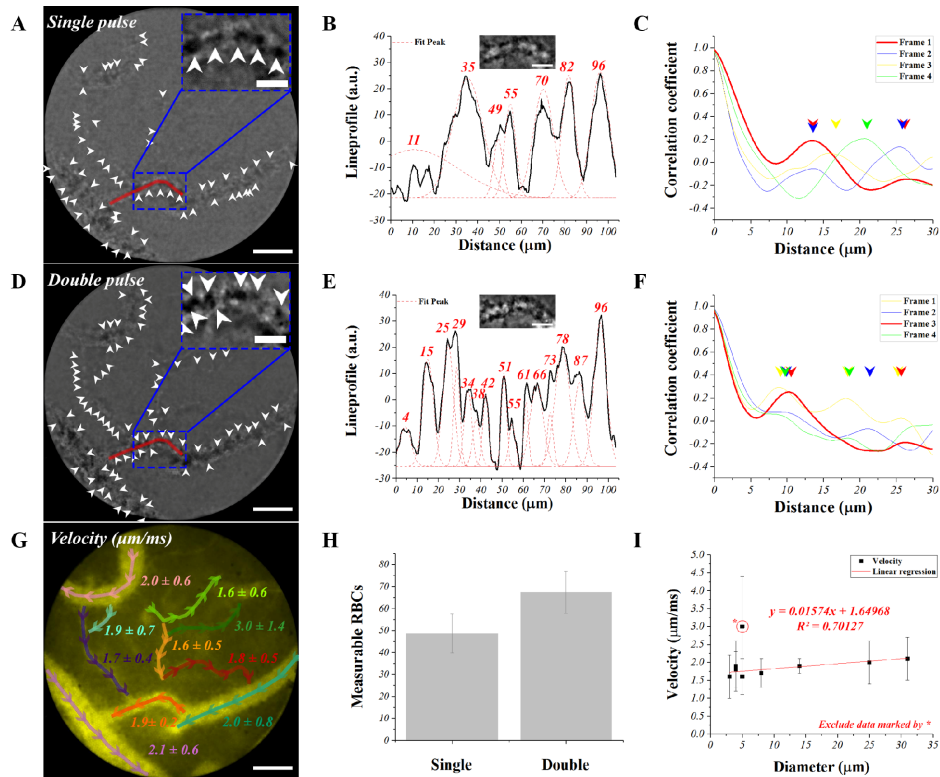

Fig. 5. Autocorrelation measurements of fluorescent cerebrovascular image using a single-pulse laser illumination method and a double-pulse laser illumination method, and blood flow measurement using a double-pulse laser illumination method. (A) Fluorescent cerebrovascular image after the enhancement process obtained using a single-pulse laser illumination method. White arrowheads indicate individual RBCs (n = 62). (B) Line profile data obtained in a red scan line of the image A. Cropped, magnified and inverted image of target blood vessel area of image a is displayed the upper center position. Red dashed lines represent the peak curves of the graph, and red digits indicate the positions of RBCs. (C) Autocorrelation measurement of line profile data obtained in 4 frames using the same position scan line as the image A (Frame 1). The arrows indicate the displacement point measured in each frame. Red arrowheads: 14 μm and 27 μm at frame 1, blue arrowheads: 14 μm and 26 μm at frame 2, yellow arrowhead: 16 μm at frame 3, and green arrowhead: 21 μm at frame 4. (D) Fluorescent cerebrovascular image after the enhancement process obtained using a double-pulse laser illumination method. White arrowheads indicate individual RBCs (n = 77). (E) Line profile data obtained in a red scan line of the image D. Cropped, magnified and inverted image of target blood vessel area of the image D is displayed in the upper center position. Red dashed lines represent the peak curves of the graph, and red digits indicate the positions of RBCs. (F) Autocorrelation measurement of line profile data obtained in 4 frames using the same position scan line as the image D (Frame 3). The arrows indicate the displacement point measured in each frame. Yellow arrowheads: 9 μm, 18 μm, and 25 μm at frame 1, blue arrowheads: 9 μm and 21 μm at frame 2, red arrowheads: 10 μm and 26 μm at frame 3, and green arrowheads: 8 μm and 18 μm at frame 4. (G) The blood flow map of the cerebral blood vessels distributed over the field of view obtained using the double-pulse laser illumination method. Each color distinguishes blood vessels, and arrows indicate the direction of blood flow. (H) Comparison of the number of measurable RBCs at 10 frames in single-pulse laser illumination method and the double-pulse laser illumination method. (I) Comparison of the measured flow velocity and diameter of the cerebral blood vessels in the image G. Pulse duration was 1 ms. Pulse interval was 5 ms in double pulse laser illumination method. Exposure time was 100 ms. Frame interval was 100 ms. The 532-nm laser output intensity was 100 mW/mm^2. Scale bars: (A, D, and G) 50 μm, (B, E) 20 μm.

3.3 CBF velocity and autocorrelation measurement using the double-pulse laser illumination method

We had determined the appropriate laser pulse duration for measuring the RBC flow as 1 ms, through previous experimental results obtained using a single-pulse laser illumination method. However, the blood-flow velocity cannot be obtained simply by just using the location information of individual RBCs. In general, the RBC velocity (v) can be calculated using the difference in position (Δx) of the observed RBCs in successive frames with frame interval (Δt_0) [40]. However, when using an imaging system with a long frame-to-frame interval of 100 ms, as in our system, it is very difficult to track the exact flow of the target RBC by observing successive frames. On the other hand, by using the double-pulse laser illumination method, one frame image can be acquired through two laser pulse exposures with a short laser pulse interval during the exposure of the CCD camera. Therefore, the RBC velocity (v) can be obtained by measuring only the displacement difference (Δx) of the RBCs generated during the laser pulse interval (Δt_0) using only one frame obtained by the double-pulse laser illumination method.

In the fluorescent cerebral blood-vessel image obtained by the double-pulse laser illumination method, nonmoving objects such as noncontractile blood vessels or surrounding tissues become clearer during the exposure of the two laser pulses, and moving objects such as RBCs appear as overlapped particle pairs. In practice, as shown in Fig. 5(H), the average number of measurable RBCs measured using 10 frames increased by approximately 1.4 times from 49 ± 9 for single-pulse illumination (Fig. 5(A)) to 67 ± 9 for double-pulse illumination (Fig. 5(D)). RBC tracking was possible only when using enhanced fluorescence images marked with white arrowheads, and the blood-flow velocity could be calculated by measuring the distance between RBC pairs.

However, in order to numerically compare the repetition interval of RBCs in the fluorescence images measured by the double-pulse laser illumination method and single-pulse laser illumination method, the autocorrelation was first measured before the blood-flow velocity measurement (Fig. 5(C) and 5(F)). The line intensity profiles of the pixels measured using a scan line with specific dimensions, using the final enhanced fluorescence images used for RBC tracking, had a relatively bright intensity value in the fluorescence-labeled plasma than those of the fluorescently unlabeled RBCs of a target blood vessel. The intensity profile curves were inverted and normalized to better identify the locations of RBCs displayed as dark areas. The inverted and normalized images had relatively bright intensity values in the RBCs than in the plasma, and in the inverted and normalized line profile curves of 5D and 5E, the RBC positions were located at the peaks of the normalized line profile curve graphs. In addition, red dashed lines represented the peak curves of the graph, and red digits indicated the positions of RBCs. For clarity, the cropped and magnified image with the pixel intensity inversion was placed at the top center of the normalized line profile curve graph.

In general, in PIV research, cross correlation techniques are applied to determine the RBC velocity by measuring the density pattern and plasma spacing of RBCs that remain constant in the microvessels [26–28, 33, 40]. Similarly, we can measure the density pattern of constantly maintained RBCs by using the single-pulse laser illumination method (Fig. 5(C)). The autocorrelation can be measured using the line profile data obtained in four frames using the red scan line at the same position shown in Fig. 5(A). Autocorrelation curves are represented by the color representing the measured frame numbers, and the arrowheads indicate the displacement points (i.e., the density pattern of constantly maintained RBCs or the plasma spacing between RBCs) measured in each frame: 14 μm and 27 μm for frame 1, 14 μm and 26 μm for frame 2, 16 μm for frame 3, and 21 μm for frame 4.

The autocorrelation coefficient measured using the single-pulse laser illumination method represents the density pattern of the RBCs, and the autocorrelation coefficient measured using the double-pulse laser illumination method includes the moving distance information of the same RBC with a constant interval. As shown in Fig. 5(F), the autocorrelation coefficient curves measured using the double-pulse laser illumination method have a peak point close to that of the single-pulse laser illumination method: 9 μm, 18 μm, and 25 μm in frame 1, 9 μm

and 21 µm in frame 2, 10 µm and 26 µm in frame 3, and 8 µm and 18 µm in frame 4. The first peak point is determined by the repeat displacement of the RBC pairs, but the second peak point is ignored because the displacement is too long to be determined by the interval of the RBC pairs. In the autocorrelation obtained by the double-pulse laser illumination method, the peak point of the autocorrelation, which is equal to or greater than the peak value of the autocorrelation of the single-pulse laser illumination method can be ignored because it is longer than the distance between the RBC pairs.

In this double-pulse laser illumination method using a laser pulse interval of 5 ms (Δt_0), the repeat displacement of the RBC pairs measured by autocorrelation is $\Delta \mathbf{x}$, and the velocity (v) at this time can be calculated according to Eq. (1). The measured blood-flow velocities based on autocorrelation measurements are as follows: 1.8 µm/ms in frame 1, 1.8 µm/ms in frame 2, 2 µm/ms in frame 3, and 1.6 µm/ms in frame 4.

The autocorrelation result shows not only the displacements between RBC pairs but also the displacements between other RBCs because the total interval to calculate the autocorrelation is short, and a probabilistic analysis can be performed using a limited number of RBCs obtained from in vivo experiments.

As shown in Fig. 5(I), except for data marked with asterisks (*3.0 ± 1.4 µm/ms at 5 µm (n_{pair} = 23)), there is a significant linear correlation in the graph of flow velocity versus cerebrovascular diameter measured in Fig. 5(G) (r = 0.8374, p<0.05).
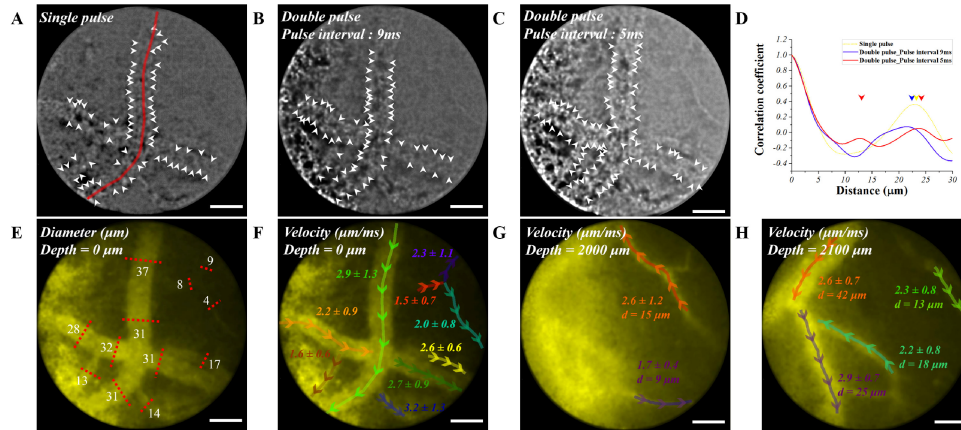

Fig. 6. Autocorrelation measurement with pulse interval of double-pulse laser illumination method and comparison of cerebral blood flow measurement at various depths using final protocol of a double-pulse laser illumination method. (A) Fluorescent cerebrovascular image after the enhancement process obtained using a single-pulse laser illumination method. Red line is the scan line that measures the intensity profile. White arrowheads indicate individual RBCs (n = 70). (B) Fluorescent cerebrovascular image after the enhancement process obtained using a double-pulse laser illumination method with a pulse interval of 9 ms (n = 71). (C) Fluorescent cerebrovascular image after the enhancement process obtained using a double-pulse laser illumination method with a pulse interval of 5 ms (n = 81). (D) Autocorrelation measurement of line profile data obtained using the scan line as in the image A. The arrows indicate the displacement point measured in each frame. Yellow arrowheads: 23 µm in single-pulse laser illumination method. Blue arrowhead: 22 µm in double-pulse laser illumination method with a pulse interval of 9 ms, and red arrowhead: 13 µm and 24 µm in double-pulse laser illumination method with a pulse interval of 5 ms. (E) Distribution of blood vessel diameter on the brain surface. (F) Blood flow map of the surface cerebral blood vessels distributed over the field of view obtained using a double-pulse laser illumination method. Each color distinguishes blood vessels, and arrows indicate the direction of blood flow. (G) Distribution of blood vessel diameter and blood flow in the brain depth of 2000 µm. (H) Distribution of blood vessel diameter and blood flow in the brain depth of 2100 µm. Pulse duration was 1 ms. Pulse interval was 9 ms in (B), 5 ms in (B, F–H). Exposure time was 10 ms. Frame interval was 100 ms. The 532-nm laser output intensity was 100 mW/mm². Scale bars: (A–C, E–H) 50 µm.

Finally, the blood-flow velocities according to the diameter of the blood vessels measured by the double-pulse laser illumination method with a pulse width of 1 ms and a pulse interval of 5 ms are as follows. The blood-flow velocities are listed in order from left to right and top to bottom on a diameter basis as shown in Fig. 4(A) (Fig. 5(G)), total number of RBC pairs (n_{pair}) = 281): 2.0 ± 0.6 μm/ms at 25 μm (n_{pair} = 21), 1.6 ± 0.6 μm/ms at 3 μm (n_{pair} = 31), 1.9 ± 0.7 μm/ms at 4 μm (n_{pair} = 11), *3.0 ± 1.4 μm/ms at 5 μm (n_{pair} = 23), 1.7 ± 0.4 μm/ms at 8 μm (n_{pair} = 32), 1.6 ± 0.5 μm/ms at 5 μm (n_{pair} = 24), 1.8 ± 0.5 μm/ms at 4 μm (n_{pair} = 37), 2.1 ± 0.6 μm/ms at 31 μm (n_{pair} = 23), 1.9 ± 1.2 μm/ms at 14 μm (n_{pair} = 24), and 2.0 ± 0.8 μm/ms at 28 μm (n_{pair} = 55).

3.4 Comparison of autocorrelation measurements according to the pulse interval of a double-pulse laser and measurement of CBF from brain surface to the deep brain using the double-pulse laser illumination method

In the double-pulse laser illumination method, the pulse interval is as important as the laser pulse period. When measuring the blood-flow velocity, the laser pulse interval of the double-pulse laser system is treated the same as the frame interval of a single-pulse laser system or a high-frame-rate measurement system. Thus, the double-pulse laser illumination method using a long laser pulse interval finds it relatively difficult to find RBC pairs because the paths of the RBCs that moved during the interval are long, similar to that in a general blood-flow imaging system with a slow frame interval. The fluorescence images of blood vessels were obtained using the single-pulse laser illumination method and double-pulse laser illumination method, both using a pulse duration of 1 ms with 10 ms exposure time (Fig. 6(A–C)). At the same time, the fluorescence images using the double-pulse laser illumination method were compared for laser pulse intervals of 5 ms and 9 ms, respectively.

The autocorrelation was measured using the respective inverted and normalized line profile data obtained by the red scan line at the same position shown in Fig. 6(A). In this experiment, the density patterns of the constantly maintained RBCs could also be measured using the single-pulse laser illumination method (Fig. 6(D)). The colors of the correlation curves indicate the autocorrelation coefficients obtained from the single-pulse laser illumination method and the double-pulse laser illumination method with laser intervals of 9 ms and 5 ms, respectively. The arrowheads indicate the displacement points: 23 μm for the single-pulse laser illumination method, 22 μm for the double-pulse laser illumination method using 9 ms laser interval, and 13 μm and 24 μm for the double-pulse laser illumination method using the 5 ms laser interval.

A broad peak point of 22 μm, similar to the displacement of 23 μm obtained from single-pulse data, was obtained by the double-pulse laser illumination method using a 9 ms laser interval. This means that the repetitive interval of a pair of RBCs considered as the same RBC in a double-pulse exposed fluorescence image measured at a laser interval of 9 ms is similar to the density interval between the different RBCs in the blood vessel. We concluded that it is difficult to measure blood flow using a dual-exposure laser method with a 9 ms laser pulse interval and that an appropriate laser pulse interval shorter than 9 ms should be used for RBC pair measurements.

Depending on the experiment, it may be preferable to use a short pulse interval of less than 2 ms, but it is very important to choose the appropriate pulse interval to measure the distance of a sufficiently distinguishable pair of RBCs. If the distance of a pair of RBCs is shorter than the resolution of the measurement system, it will be difficult to measure the blood flow as the two RBCs cannot be distinguished because of insufficient movement of the RBCs during the short pulse interval. Pulse imaging systems with a resolution of 2 μm, similar to our system, require a pulse interval of 2 ms or more when measuring 2 mm/s of blood flow using the double-pulse laser illumination method. Experimental data were not presented, but it was difficult to measure the spacing of specific RBC pairs when experiments were performed at intervals of 2 ms. Experimentally, the pulse interval of 5 ms was applied to all blood-flow velocities measured using the double-pulse laser illumination method, because this pulse interval was found to be suitable for measuring RBC density, plasma fluorescence

intensity, and vessel diameter, in this study. The single-pulse laser illumination method could also be used to measure the blood-flow velocity by tracking the flow path of RBCs observed in an oval shape. However, it may be difficult to distinguish it from RBC clustering because of the similar oval shapes of the flow paths of individual RBCs (Fig. 4(H)).

In our system, the measurable range of RBC velocity can be predicted by numerical calculations. When using the double-pulse laser illumination method with a 1 ms laser pulse duration and a 5 ms laser pulse interval, the calculated measurable range of RBC velocity is 0.4 μm/ms–60 μm/ms over a pair RBC distance of 2–300 μm, respectively. Blood-flow velocities below this range indicate stagnant flow, and velocities beyond this range cannot be measured.

The autocorrelation measured at the 5 ms pulse interval is 13 μm and the autocorrelation-based blood flow measured is 2.6 μm/ms.

Finally, the blood-flow velocities according to the diameter of the blood vessels, measured directly using the double-pulse laser illumination method, are as follows (Fig. 6(E–F), total n_{pair} = 283). The blood-flow velocities are listed in the order of vessel diameter: 2.0 ± 0.8 μm/ms at 4 μm (n_{pair} = 20), 1.5 ± 0.7 μm/ms at 8 μm (n_{pair} = 12), 2.3 ± 1.1 μm/ms at 9 μm (n_{pair} = 7), 1.6 ± 0.6 μm/ms at 13 μm (n_{pair} = 25), 3.2 ± 1.3 μm/ms at 14 μm (n_{pair} = 8), 2.6 ± 0.6 μm/ms at 17 μm (n_{pair} = 17), 2.2 ± 0.9 μm/ms at 28 μm (n_{pair} = 61), 2.7 ± 0.9 μm/ms at 31 μm (n_{pair} = 27), and 2.9 ± 1.3 μm/ms at 37 μm (n_{pair} = 106).

Additionally, since our old fiber-bundle-based imaging platform was ultimately designed to enable fluorescence imaging at any location, from the superficial to the deep brain, this functionality is equally applicable to the new optical platform. Therefore, we also measured the blood-flow velocities under the deep brain using the new optical platform.

As shown in Fig. 6(E–H), fluorescence blood-vessel imaging of the live mouse brain was conducted at depths of 2 mm and 2.1 mm from the surface in the same x-y stereomicroscopic coordinate of Fig. 6(F).

The blood-flow velocities and blood-vessel diameters distributed over the entire field of view of the fluorescent blood vessel images, measured according to the depth by the double-pulse laser illumination method of the same protocol, are as follows. The blood-flow velocities are listed in the order of vessel diameter: (i) depth of 2000 μm (total n_{pair} = 52): 2.6 ± 1.2 μm/ms at 15 μm (n_{pair} = 30), 1.7 ± 0.4 μm/ms at 37 μm (n_{pair} = 22). (ii) Depth of 2100 μm (total n_{pair} = 108): 2.3 ± 0.8 μm/ms at 13 μm (n_{pair} = 17), 2.2 ± 0.8 μm/ms at 18 μm (n_{pair} = 34), 2.9 ± 0.7 μm/ms at 25 μm (n_{pair} = 32), and 2.6 ± 0.7 μm/ms at 42 μm (n_{pair} = 25).

4. Discussion

To measure the velocity of fast CBF, we adopted the PIV method instead of using a high-speed camera. With the PIV method, we could flexibly change the system according to the situation by replacing or adding the light source of the existing system, which was more economical than adding a high-speed video camera because the latest low-cost and compact high-power CW lasers could be used.

The optical platform also distinguished the proposed system from other blood-flow measurement systems with limited frame-rate dependences because it could measure faster and slower blood-flow velocities using a variety of adjustable laser parameters, depending on the experimental conditions.

As can be seen from the experimental results in Fig. 4(K), the laser pulse duration capable of measuring the maximum number of RBCs in capillaries of diameter 4 μm was 200 ms. On the other hand, other larger diameter blood vessels required a shorter pulse duration of less than 10 ms. In addition, the measurement of RBC velocities in large blood vessels up to a diameter of 30 μm was easily accomplished by using a shorter laser pulse duration of 1 ms.

However, it was difficult to identify the RBC movements in blood vessels with diameters larger than 30 μm, owing to overlapping and misidentification of RBCs because of the high densities of RBCs and fluorescent plasma.

These results are probably due to the use of a 300 mW 532-nm DPSS CW laser that is not strong enough. Using a laser light source with a laser output greater than 300 mW will allow

faster blood-flow measurements in larger vessels with dense particles such as RBCs and fluorescent molecules in plasma using short pulse durations.

In our experiment, we used contrast fluorescence images based on labeled plasma and unlabeled RBCs. In this case, in blood vessels larger than 40 μm in diameter, fast blood flow and dense particles such as RBCs and fluorescence molecules in plasma created difficulties in visualizing and tracking RBCs that appeared as dark features. To overcome this limitation, fluorescence-labeled RBCs or microspheres labeled with fluorescent dyes could be used with our optical platform to improve the visualization and tracking of fluorescence-labeled targets by enhancing the contrast ratio between labeled RBCs or microspheres and nonfluorescent backgrounds [11, 12, 24].

In practice, we were able to measure blood-flow velocities ranging from 1.5 μm/ms to 3.2 μm/ms in blood vessels ranging from 4 μm to 42 μm in diameter. The range of blood-flow velocity is a fast CBF velocity that cannot be measured with conventional low-speed imaging techniques. Our experimental results show that the proposed platform with a frame rate of 5 fps using the double-pulse laser illumination method can measure fast blood flow, which was difficult to measure with conventional low-speed imaging techniques.

In our experiment, we used a local spatial autocorrelation technique, which yielded translational displacement data directly [26–28, 33, 40]. The density patterns of RBCs in the microvessels and the plasma spacing between them remained stable at short distances, providing an autocorrelation method to measure RBC velocity. The proposed method of spatial correlation analysis based on PIV is used in many applications [27, 28, 40]. This method is effective for tracking RBCs in blood vessels with turbulent flow, such as large arteries, and can therefore be used in our optical platform to obtain displacement vectors within the vessels, in the future.

Previously, we had developed a fiber-bundle-based integrated platform for studying cerebral blood vessels in the deep brain of live animals. Owing to the unique nature of the fiber-bundle-based optical platform, the proposed platform was able to measure the entire velocity field and vascular distribution in the deep brain of live mice. The proposed technique can become a promising tool for monitoring the blood redistribution in the microcirculatory networks in the deep brain [19, 20].

In addition, the optical platform can optically stimulate the vasoconstriction of cerebral vessels during real-time fluorescence imaging, simultaneously. With optogenetic technology and this platform, this experimental method can also be applied to studies of vasoconstriction induced by optical stimulation in a SM22-ChR2 transgenic mouse expressing ChR2 in smooth muscle cell membranes [21, 41]. In cerebrovascular disease studies, vasoconstriction is an especially important vascular response for studying vascular occlusion, hemostasis, and neurovascular circuits [2, 36, 37, 42, 43].

Our experimental results demonstrated that the proposed technique could be a promising tool for CBF studies requiring real-time full-field cellular-resolution fluorescence imaging with temporal and spatial resolutions, while simultaneously measuring fast CBF velocities. Studies on flow velocity distributions are related to aging and cerebrovascular disorders with neurovascular dysfunctions in live animals [44, 45]. Thus, this method can be applied to the visualization and quantification of microcirculatory flow velocity distributions of all organs, which are extensively applied to basic and clinical studies on tissue microcirculation.

Finally, the proposed optical platform can also be used for behavioral studies on live animals, as well as for monitoring neural activity using a variety of fluorescence-based methods such as those using fluorescent organic-encoded activity indicators and gene-encoded calcium indicators [15, 23, 46, 47].

5. Conclusion

We developed a new optical platform that combined our previously developed fiber-bundle-based integrated platform and a double-pulse 532-nm laser illumination system to measure the fast CBF velocity in the blood vessels located from the surface to the deep brain of live animals. The new platform was successfully used to image cerebral blood vessels from 4 μm

to 42 μm in diameter, in anesthetized mice, and obtain CBF velocities up to 3.2 μm/ms throughout the microscope field of view of 330 μm. The developed intravital-microscope–type optical platform could be used to obtain the CBF velocity maps according to the distribution of blood vessel diameters at a depth of 2.1 mm from the brain surface in live mice. The optical platform could measure various velocities over a wide range of image conditions without adding supplementary devices or increasing the system size, by using the PIV method. Our experimental results demonstrated that the proposed technique could be a promising tool for CBF studies requiring real-time full-field cellular-resolution fluorescence imaging with temporal and spatial resolutions, while simultaneously measuring fast CBF velocities. The probe of the optical platform was also minimally invasive, flexible, and lightweight, making it suitable for behavioral studies on live animals. Furthermore, the developed optical platform could be applied to the study of cerebrovascular diseases or hemodynamics in live animal functional unit connections such as the neurovascular or gliovascular units.

Funding

Disclosures

The authors declare that there are no conflicts of interest related to this article.